ISES International Solar Energy Society

Conference Proceedings

EuroSun 2016
Palma de Mallorca (Spain), 11 – 14 October 2016

Constrained Multi-Objective Optimization of Thermocline Packed-Bed Thermal Energy Storage Systems

Jan Marti[1], Lukas Geissbühler[1], Viola Becattini[1], Andreas Haselbacher[1], Aldo Steinfeld[1]

[1] Department of Mechanical and Process Engineering, ETH Zurich, 8092 Zurich, Switzerland

Abstract

A constrained multi-objective optimization approach is used to optimize the exergy efficiency and material costs of thermocline packed-bed thermal energy storage systems. The storage height, top and bottom radii, insulation-layer thickness, and particle diameter were chosen as design variables. The competing objectives of maximizing the exergy efficiency and minimizing the material costs are dealt with by forming a Pareto front. The Pareto front allows the identification of the most efficient design for a given cost and is an important tool in the design of thermal energy storage systems. Constraints are imposed to obtain storage systems with a specified capacity. The optimization approach is applied to identify the influence of various design variables on the exergy efficiency and the material costs. The results show that a storage shaped like a truncated cone with the smallest cross-section on top has a higher exergy efficiency than common designs with a cylindrical shape or a truncated cone with the largest cross-section on top. The basic thermodynamic mechanisms leading to this superior performance are identified with detailed information about the axial temperature distribution in the packed bed and thermal losses through the structure and insulation materials.

Keywords: *thermal energy storage, thermocline energy storage, packed bed, exergy efficiency, multi-objective optimization, Pareto optimality, Pareto front*

1. Introduction

Thermal energy storage (TES) systems are required when there is a time difference between the availability and demand of thermal energy. Examples are concentrated solar power (CSP) [1] and advanced adiabatic compressed air energy storage (AA-CAES) plants [2]. CSP plants have an irregular power input due to the time-dependent nature of solar radiation and require TES to control the electricity output by partially decoupling electricity production from solar radiation. AA-CAES plants store the thermal energy produced during compression in a TES and use the stored energy later to reheat the air before expansion in a gas turbine. For both CSP and AA-CAES plants, the integration of a TES improves the system efficiency and the competitiveness on the electricity market [2, 3]. Especially thermocline TES systems using a packed bed of rocks as sensible storage material are suitable because they require only low-cost storage materials and have been shown to have high thermal efficiencies [4, 5].

The design of TES systems requires an accurate and efficient numerical model. A TES system is characterized by a large number of design variables and may need to satisfy several constraints and objectives. Tab. 1 lists the operational, geometrical, thermophysical, and performance parameters of a general TES system. The operational parameters are in general defined by the application in CSP or AA-CAES plants, the values of the geometrical parameters are usually arbitrary but need to satisfy structural constraints, the thermophysical parameters depend usually on the temperature and pressure (and therefore the operational parameters), and the performance parameters are used to compare and characterize TES systems. The large number of geometric parameters can lead to very large number of design combinations. For example, considering ten values each of the storage height, the top and bottom radii, the two insulation layers, and the particle diameter would lead to 10^6 designs, each of which would need to be simulated long enough to reach quasi-steady-state conditions. If, in addition, a combination of three storage materials is

doi:10.18086/eurosun.2016.03.03 Available at http://proceedings.ises.org

considered, the number of simulations would increase to 10^8. Even with efficient one-dimensional numerical models, the computational cost of evaluating this many designs is prohibitive. To reduce the computational cost of finding the optimal design, a numerical optimization procedure is essential. By *optimal design*, we mean a TES design that combines high efficiency with low costs. It is important to note that it is in general not possible to identify any single design as optimal because high efficiency and low cost are usually contradictory requirements. Instead, the optimization procedure should provide a series of designs depending on the relative importance of high efficiency compared to low costs.

Tab. 1: Operational, geometrical, thermophysical, and performance parameters of general TES systems. The subscript *i* indicates that several instances of a particular parameter exist, such as multiple structural and insulation layers.

Operational parameters	Geometrical parameters	Thermophysical parameters	Performance parameters
Mass flow: $\dot{m}_c$, $\dot{m}_d$ Charge/discharge time: t_c, t_d Inflow temp.: $T_{f,\mathrm{in},c}$, $T_{f,\mathrm{in},d}$ Charge/discharge pressure: p_c, p_d	TES (packed-bed) height: H_{PB} Top/bottom radius: $r_{\mathrm{PB},t}$, $r_{\mathrm{PB},b}$ Structural thickness: $l_{\mathrm{struc},i}$ Insulation thicknesses: $l_{\mathrm{ins},i}$ Particle diameter: d_p Packed-bed porosity: ε	Thermal cond.: k_f, k_s, $k_{\mathrm{ins},i}$ Density: ρ_f, ρ_s, $\rho_{\mathrm{ins},i}$ Heat capacity: $c_{p,f}$, c_s, $c_{\mathrm{ins},i}$ Viscosity: μ_f	Charged capacity: E_c Net discharged energy: $E_{d,\mathrm{net}}$ Supplied energy: $E_{c,\mathrm{in}}$ Efficiency: η_{en}, η_{ex} Cost: C_{TES}

Several TES optimization studies were published that optimize only the thermal performance of TES systems without considering the TES costs [6, 7] or consider a multi-objective optimization approach where the TES efficiency and the costs are optimized simultaneously [8-10]. The above-mentioned publications use models with strong simplifications to predict the TES performance, such as algebraic equations to calculate the one-dimensional temperature distribution in packed-bed TES systems, together with basic optimization methods such as the direct search method to find optimal operating and design parameters. The restrictive model simplifications and basic optimization methods can be used for a rough evaluation of packed-bed TES systems. To advance the scope and improve the accuracy of TES optimization, the model must be more sophisticated to simulate realistic charging and discharging cycles. Therefore, the TES model in this work is capable of handling variable charging, discharging, and idle periods, multiple structural and insulation layers with different thicknesses, non-cylindrical TES geometries, and temperature-dependent thermophysical properties. In addition, an efficient optimization method is required to reduce the computational costs. In this work, the objective function is formed from the exergy efficiency at the quasi-steady state and the material costs. We expect the objective function to be continuous and to have a single maximum. Because reaching the quasi-steady state often requires a large number of charge-discharge cycles to be simulated, the objective function can be relatively expensive to compute. To decrease the computational cost, the number of evaluations of the objective function should be small. Therefore, the gradient-based sequential quadratic programming (SQP) algorithm is used for the optimization in this work.

The objective of the present study is to use multi-objective optimization to design packed-bed TES systems with rocks as heat-storage medium and air as heat-transfer fluid (HTF). The objective function is formed from the exergy efficiency and the material costs. The design variables include the packed-bed height, top and bottom radii, insulation-layer thicknesses, and particle diameter while the net discharged energy and the packed-bed volume are used as nonlinear constraints. The trade-off between increasing the exergy efficiency and reducing the TES material costs is demonstrated through the concept of Pareto optimality to identify optimal designs that combine a high efficiency with low costs.

2. Model and numerical method

The optimization tool is a combination of a previously developed heat-transfer model [4] and the optimization package NPSOL [11, 12]. The coupling of the heat-transfer model with the optimization package is described in [13].

2.1. TES model

The heat-transfer model can accurately predict the one-dimensional temperature distribution of packed-bed thermocline TES systems and is described in [4]. The model was verified with the exact solutions for the simplified cases of no axial conduction and wall losses during the first charging of the TES [14] and during the steady charging-discharging behavior in the limit of fast switching times [15]. Several experimental

studies were used to validate the model, including storages with rocks [5] and ceramic particles [16] using air as HTF and a storage with a combination of quartzite and sand using molten salt as HTF [17].

2.2. Optimization package

The optimization package NPSOL uses the SQP method to minimize an objective function that depends on design variables and linear and non-linear constraints [18]. The optimization problem can be formulated as

$$\text{minimize} \quad f(\vec{x}) \quad \text{subject to} \quad \vec{l} \leq r(\vec{x}) \leq \vec{u} \quad \text{with} \quad r(\vec{x}) = \begin{cases} \vec{x} \\ \bar{\bar{A}}\vec{x} \\ \vec{c}(\vec{x}) \end{cases} \tag{1}$$

where $\vec{x}$ is a vector of n design variables, $f(\vec{x})$ is the objective function, $\vec{l}$ and $\vec{u}$ are vectors with the lower and upper bounds of each design variable, $\bar{\bar{A}}$ is a $m_L \times n$ matrix describing the m_L linear constraints, and $\vec{c}(\vec{x})$ is a vector with m_N nonlinear constraint functions. The values of $\vec{l}$, $\vec{u}$, $\bar{\bar{A}}$, and the initial values of $\vec{x}$ are required as input parameters to NPSOL. The functions $f(\vec{x})$ and $\vec{c}(\vec{x})$ are calculated by the TES code described above and provided to NPSOL. Besides the function values of $f(\vec{x})$ and $\vec{c}(\vec{x})$, the SQP method requires also the gradients of $f(\vec{x})$ and $\vec{c}(\vec{x})$ with respect to each design variable.

2.2.1. Complex-step derivative approximation

To avoid the "step-size dilemma" of finite-difference methods, the complex-step derivative approximation is used [19-21]. This method uses complex calculus to calculate the derivative without subtraction and hence is unaffected by cancellation errors. This allows a very small step size to be used to reduce the truncation error and therefore the accuracy of the complex-step derivative approximation can exceed the accuracy of finite difference by several orders of magnitudes [19, 21].

To apply the complex-step derivative approximation, the floating-point variables and constants used in the TES code are converted into complex variables and constants and the intrinsic Fortran functions and operators are overloaded to handle complex arguments. The conversion process is automated by a code that adjusts all Fortran files and the overloaded intrinsic functions and operators are defined in an additional Fortran module similar to [21]. By introducing a complex step size to a specific design variable, e.g. x_1, while setting the complex part of the other design variables to zero, the complex part of the objective function $f(\vec{x})$ can be used to approximate the derivative of the objective function with respect to this particular design variable using

$$\frac{\partial f}{\partial x_1} \approx \frac{\mathrm{Im}[f(x_1 + ih, x_2, \ldots, x_n)]}{h} \tag{2}$$

where $x_{1,2,\ldots,n}$ are the design variables and h is the complex step size (typically chosen to be 10^{-12}). The same procedure can be applied to any function calculated by the converted TES code.

2.2.2. Multi-objective optimization

The objectives in multi-objective optimization are in general competing, so one objective can only be improved when at least another objective is worsened [22]. This trade-off can be visualized with the Pareto front that describes the best possible combinations of the competing objectives within the objective function space [23]. Several approaches exist to combine the competing objectives to calculate the Pareto front [24]. One of the simplest methods is the weighted-sum method in which a single objective function is calculated by combining the competing objectives according to

$$f(\vec{x}) = \sum_{i=1}^{N_o} w_i \hat{f}_i(\vec{x}) \tag{3}$$

where N_o is the total number of objectives and w_i is the relative weight of objective $\hat{f}_i(\vec{x})$. The sum of all weights is equal to unity. For competing objectives, the Pareto front can be computed by varying the weights gradually and computing for each set of weights the optimum of the weighted sum [25].

Two objective functions are considered in the present study: the exergy efficiency of one charge-discharge cycle at the quasi-steady state and the material costs of the TES. The weighted sum of these two

objective functions is given by

$$f(\vec{x}) = w(1-\eta_{\mathrm{ex}}) + (1-w)\frac{C_{\mathrm{TES}}}{C_{\mathrm{TES,ref}}} \quad (4)$$

where η_{ex} is the exergy efficiency, C_{TES} is the total material cost of the TES, and $C_{\mathrm{TES,ref}}$ is an estimation of the material cost. The normalization is used to avoid one objective function dominating the other. The exergy efficiency is defined in [4] and the material cost of the TES is computed from

$$C_{\mathrm{TES}} = \sum_{i=1}^{N_m} c_i V_i \quad (5)$$

where N_m is the total number of materials, c_i is the volumetric cost of material i, and V_i is the volume of material i. The material cost includes the storage material, the structural materials, and the insulation materials. The volumetric costs of the various materials are given in [4].

2.2.3. Non-linear optimization constraints

In the present study, two non-linear constraints are considered: the net discharged energy $E_{d,\mathrm{net}}$ and the packed-bed volume V_{PB}. The net discharged energy describes the net thermal energy extracted from the TES during discharging and is given by

$$E_{d,\mathrm{net}} = E_{d,\mathrm{out}} - E_{d,\mathrm{in}} = \int_0^{\Delta t_d} \dot{m}\left\{h_f\left(T_{d,\mathrm{out}}\right) - h_f\left(T_{d,\mathrm{in}}\right)\right\} dt \quad (6)$$

where $\dot{m}$ is the mass flow rate and h_f is the temperature-dependent enthalpy of the HTF. The volume of the packed bed is calculated with the well-known expression for a conical frustum.

3. Results

The results will be presented in two parts. In the first part, the optimization procedure is illustrated by using a simple TES configuration characterized by two design variables. This allows the objective and constraint functions to be visualized. In the second part, a pilot-scale TES, similar to that shown in [5], is optimized for several combinations of design variables. For the second part, each multi-objective optimization considers the exergy efficiency and the material costs as objective functions and uses the weighted-sum method as shown in Eq. (4) to find Pareto-optimal solutions. Each multi-objective optimization uses 9 values of the weight ($w = \{1.0, 0.99, 0.95, 0.8, 0.5, 0.2, 0.05, 0.01, 0.0\}$) to form the Pareto front. For all configurations, the TES geometry is a truncated cone with variable top and bottom radii. The structure of the TES is given by two concrete layers consisting of ultra-high performance concrete (UHPC) and low-density concrete (LDC) together with two layers of insulation material consisting of Microtherm® (MT) and Foamglas® (FG) as explained in [5]. To calculate the thermal losses through the structure and insulation layers, the outer wall of the TES is assumed to be at ambient temperature. The thermophysical properties of all structure, insulation, and thermal storage materials and the HTF are temperature-dependent as specified in [26]. Each TES simulation is run until a quasi-steady state is reached.

3.1. Visualization of optimization procedure

A simple method to visualize and examine the optimization procedure is to use one or two design variables and plot the objective and constraint functions as a function of the design variables. The visualization of the optimization procedure is done for the pilot-scale TES with a fixed packed-bed height of $H_{\mathrm{PB}} = 8$ m and the top and bottom packed-bed radii of the TES as design variables. The used model parameters are listed in Tab. 2. Fig. 1 shows contour lines of the exergy efficiency, the material costs, the net discharged energy, and the packed-bed volume, as a function of the top and bottom packed-bed radii. The visualization depicted in Fig. 1 is based on 400 quasi-steady-state TES simulations for discrete values of the design variables together with a linear interpolation routine to smooth the contour lines.

Fig. 2 shows on the left-hand side the exergy efficiency as a function of the top and bottom packed-bed radii together with the optimization iterations for different initial conditions and on the right-hand side a close-up of the computed optima together with the predicted optimum. Depending on the initial condition,

the optimizer requires between 12 and 35 iterations to reach the optimum. The computed optima differ by less than 0.01% from the optimum predicted from the interpolated results of the 400 quasi-steady-state simulations. Compared to a systematic approach with twenty discrete values for both design variables and the simulation of all design combinations, the gradient-based optimization reduces the computational cost by about 91 and 97%. This reduction will be even more significant when the number of design variables is increased.

Tab. 2: Operational and geometrical parameters of the pilot-scale TES model.

Operational parameters	charging duration, t_c	8.0 h	Geometrical parameters	void fraction, ε	0.342
	discharging duration, t_d	8.0 h		particle diameter, d_p	0.03 m
	mass flow rate, $\dot{m}_{\text{air}}$	0.75 kg/s		1st concrete layer, l_{UHPC}	0.05 m
	charging temperature, T_c	823.15 K		2nd concrete layer, l_{LDC}	0.3 m
	discharging temperature, T_d	293.15 K		1st insulation layer, l_{MT}	0.1 m
	ambient temperature, T_0	293.15 K		2nd insulation layer, l_{FG}	0.1 m

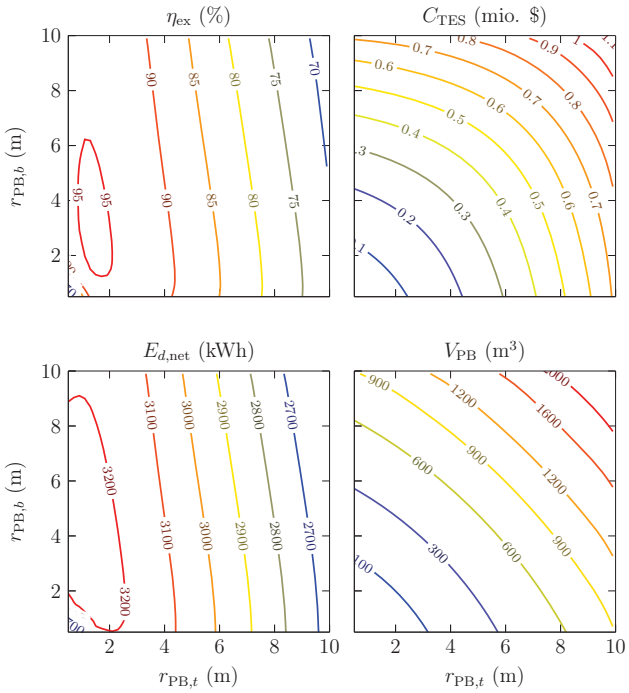

Fig. 1: Exergy efficiency, material cost, net discharged energy, and packed-bed volume as a function of the top and bottom packed-bed radii of the TES for a fixed packed-bed height of $H_{\text{PB}} = 8$ m and TES model parameters according to Tab. 2.

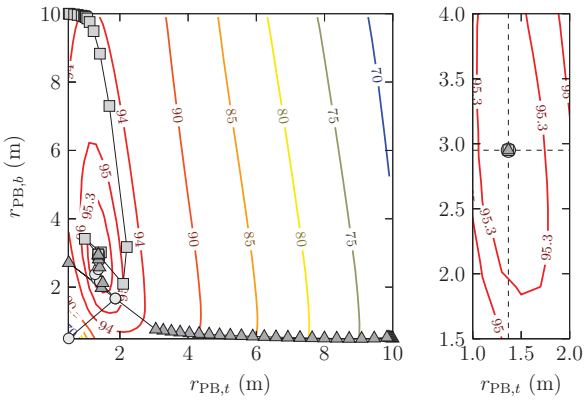

Fig. 2: Left-hand side: exergy efficiency as a function of the top and bottom packed-bed radii of the TES together with optimization iterations for different initial conditions. Right-hand side: close-up of the computed optima for all initial conditions (symbols) and the predicted optimum (dashed lines).

3.2. Pilot-scale TES

To simplify the interpretation of the multi-objective optimization results, the TES configurations have the same operating conditions but different numbers of design variables and constraints. With this approach, the influence of individual design variables on the optimization results can be pointed out. The optimization uses two nonlinear constraints and five design variables as shown in Tab. 3. The nonlinear constraints are the net discharged energy and the packed-bed volume and the design variables are the height, top and bottom radii of the packed bed, the outer insulation-layer thickness, and the particle diameter. For simplicity, the considered structure and insulation materials have on the top, bottom, and side walls of the TES the same thicknesses. Depending on the optimization configuration, the packed-bed volume and some of the design variables are fixed or variable as indicated in Tab. 3. To have a benchmark for the designs, the net discharged energy is used as constraint and must be $\mathrm{E}_{d,\mathrm{net}} \geq 3$ MWh. (For all configurations, $\mathrm{E}_{d,\mathrm{net}}$ does not exceed 3.3 MWh.)

Tab. 3: Nonlinear constraints and design variables of the pilot-scale TES optimization configurations.

Configuration		1	2	3
Nonlinear constraints	net discharged energy, $E_{d,\mathrm{net}}$	≥ 3 MWh	≥ 3 MWh	≥ 3 MWh
	packed-bed volume, V_{PB}	300 m^3	–	–
Design variables	packed-bed height, H_{PB}	8.0 m	0.5–10.0 m	0.5–10.0 m
	top radius, $r_{\mathrm{PB},t}$	0.5–10.0 m	0.5–10.0 m	0.5–10.0 m
	bottom radius, $r_{\mathrm{PB},b}$	0.5–10.0 m	0.5–10.0 m	0.5–10.0 m
	outer insulation, $t_{\mathrm{ins,out}}$	0.1 m	0.1 m	0.01–1.0 m
	particle diameter, d_p	0.03 m	0.03 m	0.001–0.1 m

3.2.1. Configuration 1

The first configuration uses $E_{d,\mathrm{net}} \geq 3$ MWh and $\mathrm{V_{PB}} = 300$ m^3 as nonlinear constraints and the top and bottom packed-bed radii as design variables. With a fixed packed-bed volume, all Pareto-optimal solutions must lie on the contour indicating a packed-bed volume of 300 m^3 in Fig. 1.

Fig. 3 depicts the TES geometries for the two extreme cases $w = 1.0$ and $w = 0.0$ together with the intermediate case $w = 0.5$ according to Eq. (4). (During charging, the HTF enters the TES from the top and exits from the bottom; during discharging, the flow direction is reversed.) The inflow and outflow ports are not indicated in Fig. 3 because they are not considered in the simulations.

For the Pareto optimal designs, a comparison of the TES material costs are presented in Fig. 4. Since the packed-bed volume is constant, the cost of the storage material is constant and the cost reduction is caused by the reduction of the required structure and insulation material. The cost of the storage material is negligible compared to the structure and insulation material. The cheapest design has a cylindrical shape because this minimizes the surface area per volume and accordingly requires the smallest amount of structure and insulation materials.

The Pareto front of the two objective functions is presented on the left-hand side of Fig. 5. The exergy efficiency can only be increased when the TES material costs is increased, which reflects the trade-off between maximizing the exergy efficiency and minimizing the material costs of a TES system. From the Pareto front, it is possible to identify the most efficient TES for a given cost and vice versa. The right-hand side of Fig. 5 shows the exergy efficiency as a function of the top and bottom radii of the packed bed. The difference between the top and bottom radii decreases with decreasing exergy efficiency while the top radius is smaller than the bottom radius until a cylindrical shape is reached. Next to the exergy efficiency, the left-hand side of Fig. 5 also presents the exergy-loss breakdown that indicates how the pumping work, thermal loss, and internal heat transfer decrease the exergy efficiency. The main decrease of the exergy efficiency results from an increase of the thermal loss while the exergy loss due to internal heat transfer stays for all designs almost constant and the required pumping power is negligible.

Fig. 6 shows on the left-hand side the net charged and net discharged exergy for each design. The net charged exergy stays constant and with a negligible exergy loss due to the required pumping power, the exergy efficiency depends mainly on the net discharged exergy. The net discharged exergy increases when the air outflow temperature during discharging increases. The comparison of the HTF outflow temperature during discharging for designs 1 and 9 is shown on the right-hand side of Fig. 6. As expected, for both designs the outflow temperature decreases during discharging while for design 1 the mean outflow

temperature is about 11 K higher than for design 9.

The mean outflow temperature during discharging is strongly influenced by the energy losses through the TES walls, particularly the top wall. Fig. 7 compares for all designs of Configuration 1 and for one charge-discharge cycle the energy losses from the storage material to the structure and insulation material through the top and side walls. When comparing the cheapest with the most efficient design, the losses increase by about 800 and 140%, respectively. This increase depends mainly on the increase of the top radius and accordingly an increase of the surface areas on the top wall and the upper part of the side wall where the temperatures and the temperature gradients to the outside are higher than in the lower section of the TES. The loss through the bottom wall is negligible compared to the top and side wall losses because the bottom wall temperature is close to the ambient temperature.

Fig. 8 shows the thermocline of the fully charged and fully discharged states for designs 1 and 9. The thermoclines of the two designs differ mainly in the upper section where the hot air enters the TES during charging. Compared to design 9, design 1 has a smaller cross-section in the upper part that leads to a higher flow velocity of the HTF and accordingly the temperature front moves further down during charging. An additional effect of the higher flow velocity is a higher Nusselt number that leads to a better interphase heat transfer.

The efficient designs in this study have, as depicted in Fig. 3, a shape like a truncated cone with the smaller cross-section on top and accordingly a negative cone angle. This shape is in contrast to existing designs that are either cylindrical [17] or have a positive cone angle [27, 28]. The trend of negative cone angles having smaller losses is consistent with the results shown in Fig. 13 of [27]. In prior works, negative cone angles appear to have not been considered because of possible drawbacks related to thermal ratcheting. Thermal ratcheting is a well-known problem of packed-bed TES systems caused by different thermal-expansion rates of the storage and structural materials. The different expansion rates can cause the storage material to settle and pack with cycling and eventually cause the storage structure to fail [29, 30]. To prevent material failure, positive cone angles have been suggested as a way to guide the expanding storage material upwards along the inclined wall and hence reduce the stresses on the storage and structural materials [27, 28]. This study does not consider mechanical stresses for simplicity. The practical implementation of a packed-bed thermocline storage with negative cone angle may require structured storage materials [31, 32] or additional material layers between the storage material and the structure to absorb the mechanical stresses [33].

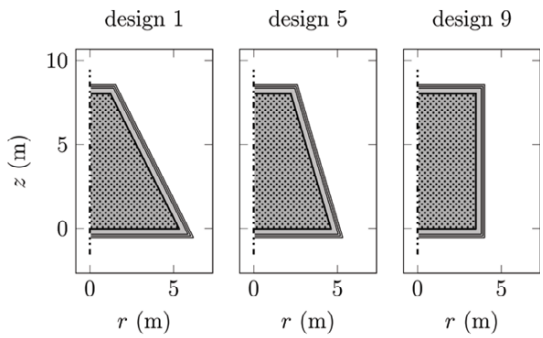

Fig. 3: Visualization of Pareto-optimal designs with w = 1.0, 0.5, and 0.0 of Configuration 1.

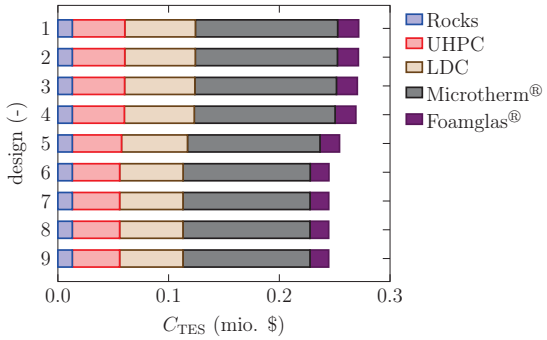

Fig. 4: Breakdown of the TES material costs for the Pareto-optimal designs of Configuration 1.

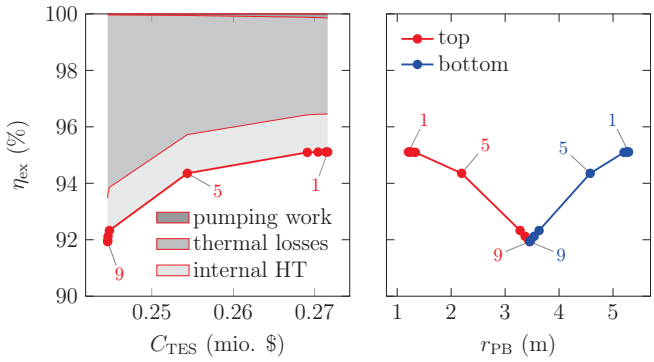

Fig. 5: Left-hand side: exergy efficiency and the exergy-loss breakdown as a function of the TES material costs. Right-hand side: exergy efficiency as a function of the top and bottom packed-bed radii of Configuration 1.

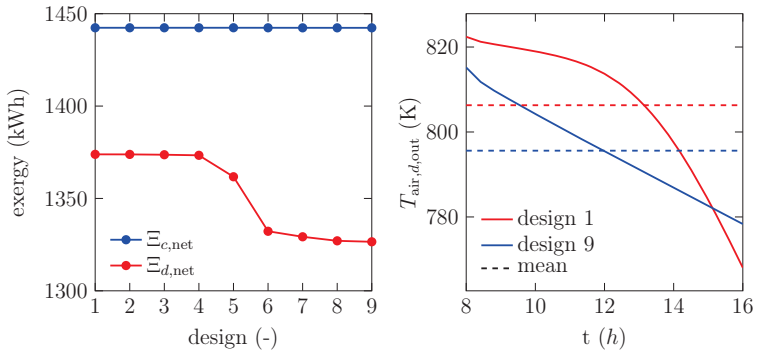

Fig. 6: Left-hand side: net charged and discharged exergies during one charge-discharge cycle for the Pareto-optimal designs. Right-hand side: HTF outflow and mean temperature during discharging for two designs of Configuration 1.

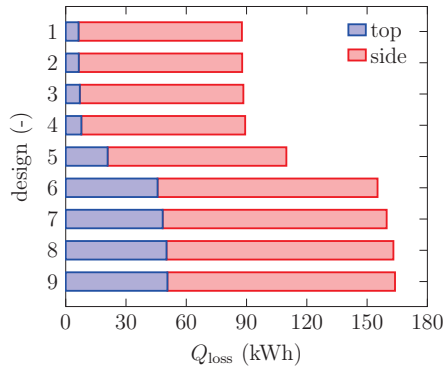

Fig. 7: Energy losses over the top and side walls from the storage material to the structure and insulation material during one charge-discharge cycle for the Pareto-optimal designs of Configuration 1.

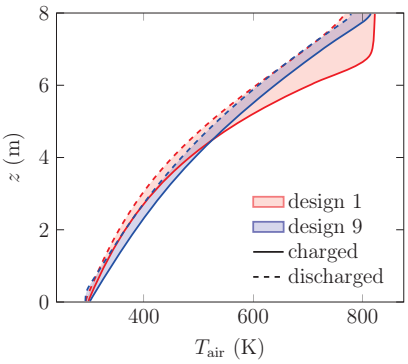

Fig. 8: Air temperature along the axial direction at fully charged and fully discharged state for two designs of Configuration 1.

3.2.2. Configuration 2

The second configuration of the multi-objective TES optimization uses $E_{d,\mathrm{net}} \geq 3$ MWh as a nonlinear constraint and the height and the top and bottom radii of the packed bed as design variables. Compared to Configuration 1, the packed-bed volume is variable. The storage geometries are depicted in Fig. 9 for the two extreme cases $w = 1.0$ and $w = 0.0$ and the intermediate case $w = 0.5$.

Fig. 10 shows the exergy efficiency as a function of the packed-bed height (left), the packed-bed volume (middle), and the material costs (right). When increasing the height, the volume and therefore the material costs increase considerably. An increased height has a favorable influence on the exergy efficiency by expanding the thermocline and reducing thereby the possibility of overcharging and overdischarging the

TES, which leads to an undesirable increase and decrease of the outflow temperatures during charging and discharging, respectively. This trend can be seen in Fig. 11 where the fully charged and discharged thermoclines of the most efficient and cheapest designs are presented. The most efficient design has temperature difference between the fully charged and discharged states of about 10 K at the top and bottom of the storage whereas the temperature differences of the cheapest design are about 200 K. Depending on the application of the TES, the minimum and maximum outflow temperatures during the charge-discharge cycle are important operational parameters that need to be considered during the design phase of the TES. For brevity, the breakdown of the TES material costs is not shown.

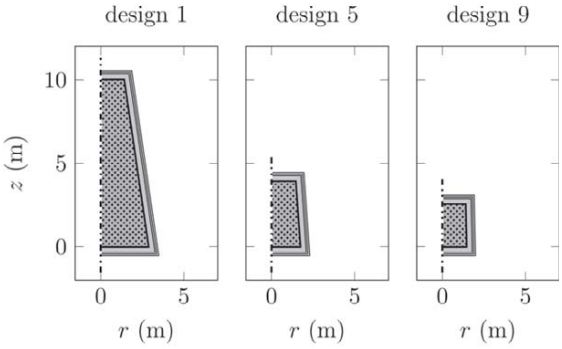

Fig. 9: Visualization of TES geometries for Pareto-optimal designs with w = 1.0, 0.5, and 0.0 of Configuration 2.

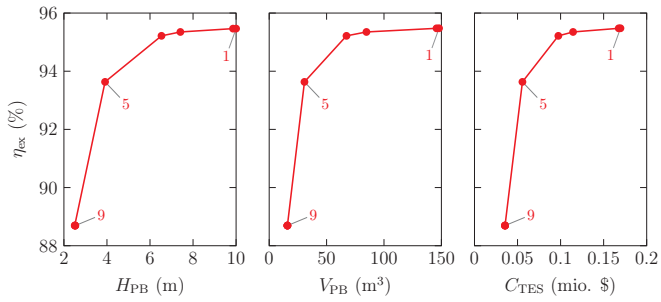

Fig. 10: Exergy efficiency as a function of the packed-bed height, pack-bed volume, and TES material costs for the Pareto-optimal designs of Configuration 2.

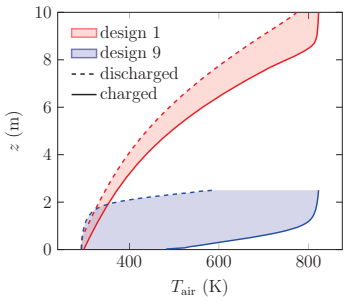

Fig. 11: Air temperature along the axial direction of the fully charged and fully discharged TES for two designs of Configuration 2.

3.2.3. Configuration 3

The third configuration of the multi-objective TES optimization uses $E_{d,\mathrm{net}} \geq 3$ MWh as a nonlinear constraint and the height, the top and bottom radii of the packed bed, the thickness of the outer insulation layer, and the particle diameter as design variables. The TES geometries for the two extreme cases $w = 1.0$ and $w = 0.0$ and the intermediate case $w = 0.5$ are depicted in Fig. 12. Compared to Configuration 2, the main difference of the TES geometries is the increased outer insulation-layer thickness of design 1.

Fig. 13 shows on the left-hand side the exergy efficiency as a function of the outer insulation-layer thickness consisting of Foamglas®. As expected, the more efficient designs have a larger insulation-layer thickness, which reaches the upper limit of 1.0 m and the lower limit of 0.01 m for the most efficient and for the cheapest designs, respectively. Increasing the insulation-layer thickness reduces the thermal losses through the top, bottom, and lateral walls but also increases the material costs as indicated on the right-hand side of Fig. 12. A breakdown of the material costs is shown in Fig. 14. For all designs, the cost for the insulation materials is the major contributor to the total TES material costs while the cost for the storage material is negligible. The four most efficient designs have an outer insulation-layer thickness between 0.66 and 1.0 m that contributes to about half of the total costs. Reducing the required amount of the insulation material is therefore essential to reduce the material costs.

Fig. 15 presents the exergy efficiency and the exergy-loss breakdown as a function of the particle

diameter. The exergy efficiency increases with increasing particle diameter. The least efficient design has a particle diameter that is equal to the lower limit of 1.0 mm while the most efficient design has a particle diameter that is 21.5 mm and therefore below the upper limit of 100.0 mm. A decreasing particle diameter influences the TES performance in two ways: it increases the heat transfer between the solid and fluid phase and it increases the pressure drop over the packed bed. An increasing heat transfer reduces thermal irreversibility and therefore increases the exergy efficiency while an increasing pressure drop increases the exergy loss due to the required pumping power and therefore decreases the exergy efficiency. The strong increase of the required pumping power for very small particles can be seen from the exergy-loss breakdown in Fig. 15. For design 9, the required pumping power is about 140 times bigger than for design 1. The increase of the heat transfer between the solid and fluid phase for a decreasing particle diameter results mainly from an increase of the specific surface area. The optimal particle diameter is therefore a trade-off between increasing the pressure drop and increasing the interphase heat transfer.

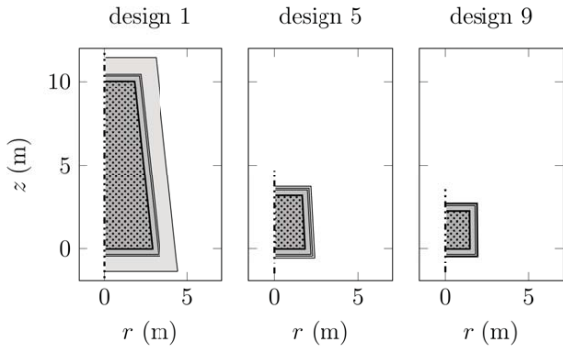

Fig. 12: Visualization of TES geometries for Pareto-optimal designs with w = 1.0, 0.5, and 0.0 of Configuration 3.

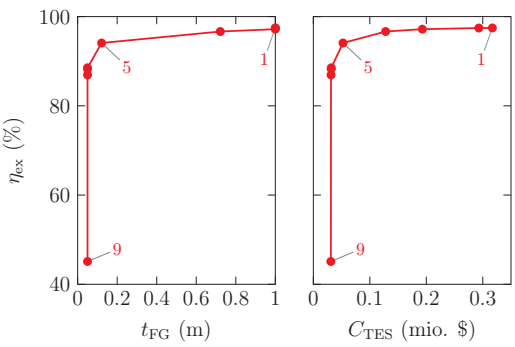

Fig. 13: Exergy efficiency as a function of the outer insulation-layer thickness (left) and the TES material costs (right) for the Pareto-optimal designs of Configuration 3

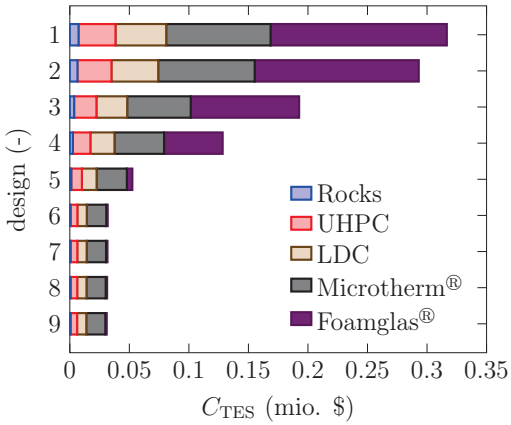

Fig. 14: TES material costs for the Pareto-optimal designs of Configuration 3.

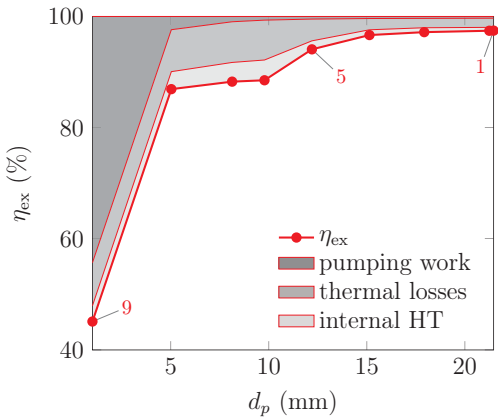

Fig. 15: Exergy efficiency and exergy-loss breakdown as a function of the particle diameter for the Pareto-optimal designs of Configuration 3.

4. Summary and Conclusions

A gradient-based multi-objective optimization method was used to optimize the exergy efficiency and the material costs of packed-bed TES systems based on their height, top and bottom radii, insulation-layer thickness, and particle diameter. Competing objectives like maximizing exergy efficiency and minimizing material costs are treated using Pareto fronts. The Pareto front shows the best possible TES designs and enables the most efficient TES for a given cost to be determined.

A systematic optimization of three pilot-scale TES configurations was used to point out the

influence of individual design variables on the exergy efficiency and material costs. In general, increasing the TES height increases the exergy efficiency but also increases the material costs. The optimization of the top and bottom radii showed that a TES design with a negative cone angle has a higher exergy efficiency than commonly used cylindrical shaped TES or designs with a positive cone angle. This results mainly from a reduced surface area in the hot upper section of the TES and therefore decreased thermal losses to the environment. The basic thermodynamic mechanisms leading to the superior performance of a TES with a negative cone angle were identified with detailed information about the axial temperature distribution in the packed bed and thermal losses through the structure and insulation materials. The potential mechanical drawbacks of a negative cone angle related to thermal ratcheting are not considered in this work but could perhaps be solved by using structured storage materials without loose particles or material layers that absorb the thermomechanical stress during charge-discharge cycles. Detailed material-cost breakdowns showed that for low-cost storage materials like rocks, a reduction of the required insulation material is essential to further reduce the TES material costs. In addition, the optimization revealed the trade-off between reducing the pressure drop and improving the interphase heat transfer when optimizing the particle diameter.

Acknowledgement

The authors gratefully acknowledge funding from the European Union's Horizon 2020 research and innovation programme under grant agreements No. 654387 (RICAS2020, www.ricas2020.eu) and 642067 (RESLAG, www.reslag.eu), from the Swiss Commission for Technology and Innovation through the Swiss Competence Center for Energy Research on Heat and Electricity Storage, from the Swiss National Science Foundation under NRP 70 grant No. 407040_153776, and from the European Union under the 7th Framework Program (grant No. 609837, STAGE-STE). The authors also acknowledge helpful discussions with Prof. R. T. Haftka from the University of Florida.

References

[1] M. Romero, A. Steinfeld, 2012. Concentrating solar thermal power and thermochemical fuels. Energy & Environmental Science. 5, 9234-9245.
[2] C. Bullough, C. Gatzen, C. Jakiel, M. Koller, A. Nowi, S. Zunft, 2004. Advanced adiabatic compressed air energy storage for the integration of wind energy, in: Proceedings of the European Wind Energy Conference, pp. 25.
[3] H.L. Zhang, J. Baeyens, J. Degrève, G. Cacères, 2013. Concentrated solar power plants: Review and design methodology. Renewable and Sustainable Energy Reviews. 22, 466-481.
[4] L. Geissbühler, M. Kolman, G. Zanganeh, A. Haselbacher, A. Steinfeld, 2016. Analysis of industrial-scale high-temperature combined sensible/latent thermal energy storage. Applied Thermal Engineering. 101, 657-668.
[5] G. Zanganeh, A. Pedretti, S. Zavattoni, M. Barbato, A. Steinfeld, 2012. Packed-bed thermal storage for concentrated solar power – Pilot-scale demonstration and industrial-scale design. Solar Energy. 86, 3084-3098.
[6] H. Torab, D.E. Beasley, 1987. Optimization of a packed bed thermal energy storage unit. Journal of Solar Energy Engineering. 109, 170-175.
[7] A.S.A. Ammar, A.A. Ghoneim, 1991. Optimization of a sensible heat storage unit packed with spheres of a local material. Renewable Energy. 1, 91-95.
[8] O. Maaliou, B.J. McCoy, 1985. Optimization of thermal energy storage in packed columns. Solar Energy. 34, 35-41.
[9] C. Choudhury, P.M. Chauhan, H.P. Garg, 1995. Economic design of a rock bed storage device for storing solar thermal energy. Solar Energy. 55, 29-37.
[10] R. Domański, G. Fellah, 1998. Thermoeconomic analysis of sensible heat, thermal energy storage systems. Applied Thermal Engineering. 18, 693-704.
[11] P.E. Gill, W. Murray, M.A. Saunders, M.H. Wright, 1986. User's Guide for NPSOL: A Fortran Package for Nonlinear Programming, in: Report SOL 86-2, Stanford University, Stanford, CA, Department of Operations Research.
[12] Stanford Business Software Inc., Stanford University, California, USA.
[13] J. Marti, L. Geissbühler, V. Becattini, A. Haselbacher, A. Steinfeld, 2016. Constrained Multi-Objective Optimization of Thermocline Packed-Bed Thermal Energy Storage Systems. in preparation.

[14] A. Anzelius, 1926. Über Erwärmung vermittels durchströmender Medien. Journal of Applied Mathematics and Mechanics/Zeitschrift für Angewandte Mathematik und Mechanik. 6, 291-294.
[15] H. Klein, G. Eigenberger, 2001. Approximate solutions for metallic regenerative heat exchangers. International Journal of Heat and Mass Transfer. 44, 3553-3563.
[16] A. Meier, C. Winkler, D. Wuillemin, 1991. Experiment for modelling high temperature rock bed storage. Solar Energy Materials. 24, 255-264.
[17] J.E. Pacheco, S.K. Showalter, W.J. Kolb, 2002. Development of a Molten-Salt Thermocline Thermal Storage System for Parabolic Trough Plants. Journal of Solar Energy Engineering. 124, 153-159.
[18] P.E. Gill, W. Murray, M.H. Wright, 1981. Practical optimization. Academic Press, London.
[19] J.N. Lyness, C.B. Moler, 1967. Numerical differentiation of analytic functions. Journal on Numerical Analysis. 4, 202-210.
[20] J.C. Newman, K.W. Anderson, D.L. Whitfield, 1998. Multidisciplinary sensitivity derivatives using complex variables. Mississippi State University Publication, MSSU-EIRS-ERC-98-08.
[21] J.R.R.A. Martins, P. Sturdza, J.J. Alonso, 2003. The complex-step derivative approximation. Transactions on Mathematical Software. 29, 245-262.
[22] A. Toffolo, A. Lazzaretto, 2002. Evolutionary algorithms for multi-objective energetic and economic optimization in thermal system design. Energy. 27, 549-567.
[23] Y. Censor, 1977. Pareto Optimality in Multiobjective Problems. Applied Mathematics and Optimization. 4, 41-59.
[24] R.T. Marler, J.S. Arora, 2004. Survey of multi-objective optimization methods for engineering. Structural and Multidisciplinary Optimization. 26, 369-395.
[25] D.W. Zingg, M. Nemec, T.H. Pulliam, 2008. A comparative evaluation of genetic and gradient-based algorithms applied to aerodynamic optimization. European Journal of Computational Mechanics/Revue Européenne de Mécanique Numérique. 17, 103-126.
[26] G. Zanganeh, 2014. High-Temperature Thermal Energy Storage for Concentrated Solar Power with Air as Heat Transfer Fluid, in, Diss. Eidgenössische Technische Hochschule ETH Zürich, Nr. 21802.
[27] G. Zanganeh, A. Pedretti, A. Haselbacher, A. Steinfeld, 2015. Design of packed bed thermal energy storage systems for high-temperature industrial process heat. Applied Energy. 137, 812-822.
[28] K.Y. Wang, R.E. West, F. Kreith, P. Lynn, 1985. High-temperature sensible-heat storage options. Energy. 10, 1165-1175.
[29] S. Flueckiger, Z. Yang, S.V. Garimella, 2011. An integrated thermal and mechanical investigation of molten-salt thermocline energy storage. Applied Energy. 88, 2098-2105.
[30] A. Dogangun, Z. Karaca, A. Durmus, H. Sezen, 2009. Cause of Damage and Failures in Silo Structures. Journal of Performance of Constructed Facilities. 23, 65-71.
[31] J.E. Skinner, M.N. Strasser, B.M. Brown, R. Panneer Selvam, 2013. Testing of High-Performance Concrete as a Thermal Energy Storage Medium at High Temperatures. Journal of Solar Energy Engineering. 136, 021004.
[32] S. Zunft, M. Hänel, M. Krüger, V. Dreißigacker, 2014. A Design Study for Regenerator-type Heat Storage in Solar Tower Plants–Results and Conclusions of the HOTSPOT Project. Energy Procedia. 49, 1088-1096.
[33] Z. Chang, X. Li, C. Xu, C. Chang, Z. Wang, Q. Zhang, Z. Liao, Q. Li, 2016. The effect of the physical boundary conditions on the thermal performance of molten salt thermocline tank. Renewable Energy. 96, 190-202.